Journal of Vacuum Science and Technology B

RESEARCH ARTICLE | FEBRUARY 05 2024

Excitonic effects in the optical absorption of gapless semiconductor α-tin near the direct bandgap

Stefan Zollner

J. Vac. Sci. Technol. B 42, 022203 (2024)
https://doi.org/10.1116/6.0003278

View Online
Export Citation
CrossMark

05 February 2024 16:56:57

JVST B
Journal of Vacuum Science & Technology B

ARTICLE

pubs.aip.org/avs/jvb

Excitonic effects in the optical absorption of gapless semiconductor α-tin near the direct bandgap

Cite as: J. Vac. Sci. Technol. B **42**, 022203 (2024); doi: 10.1116/6.0003278
Submitted: 4 November 2023 · Accepted: 5 January 2024 ·
Published Online: 5 February 2024

View Online

Export Citation

CrossMark

Stefan Zollner[a)]

AFFILIATIONS

Department of Physics, New Mexico State University, MSC 3D, PO Box 30001, Las Cruces, New Mexico 88003-8001

Note: This paper is part of the 2024 Special Topic Collection on Developing SiGeSn Technology: Materials and Devices.
[a)]**Author to whom correspondence should be addressed:** zollner@nmsu.edu. URL: http://femto.nmsu.edu

ABSTRACT

Most cubic semiconductors have threefold degenerate p-bonding valence bands and nondegenerate s-antibonding conduction bands. This allows strong interband transitions from the valence to the conduction bands. On the other hand, intervalence band transitions within p-bonding orbitals in conventional p-type semiconductors are forbidden at $k = 0$ and, therefore, weak, but observable. In gapless semiconductors, however, the s-antibonding band moves down between the split-off hole band and the valence band maximum due to the Darwin shift. This band arrangement makes them three-dimensional topological insulators. It also allows strong interband transitions from the s-antibonding valence band to the p-bonding bands, which have been observed in α-tin with Fourier-transform infrared spectroscopic ellipsometry [Carrasco *et al.*, Appl. Phys. Lett. **113**, 232104 (2018)]. This manuscript presents a theoretical description of such transitions applicable to many gapless semiconductors. This model is based on $\vec{k}\cdot\vec{p}$ theory, degenerate carrier statistics, the excitonic Sommerfeld enhancement, and screening of the transitions by many-body effects. The impact of nonparabolic bands is approximated within Kane's $8\times 8\,\vec{k}\cdot\vec{p}$-model by adjustments of the effective masses. This achieves agreement with experiments.

Published under an exclusive license by the AVS. https://doi.org/10.1116/6.0003278

05 February 2024 16:56:57

I. INTRODUCTION

Due to relativistic effects, the energy of the s-antibonding Γ_2' (or Γ_7^- in the double group notation) band in diamond-type semiconductors decreases relative to the top of the Γ_{25}' (or Γ_8^+) valence band maximum with increasing atomic number. This is known as the Darwin shift.[1,2] (It can also be found in zinc blende semiconductors like HgTe, but the character notations of their space group T_d^2 differ from the diamond group O_h^7.) The difference $E_0 = E_{7^-} - E_{8^+}$ between these two energy levels becomes negative for α-tin, where the Γ_7^- band is situated between the Γ_8^+ valence band maximum and the Γ_7^+ split-off hole band. For symmetry reasons, the bandgap of α-tin is, therefore, exactly zero, making it a semimetal. The lower Γ_8^+ band forms the heavy hole valence band, while the upper Γ_8^+ band (with the same symmetry as the light hole band in Ge) forms the conduction band.[3–9] See Fig. 1 for a schematic of the band structure.

Such inverted or gapless semiconductors have been studied for many years.[1,2] Other examples include $Ge_{1-x}Sn_x$ alloys with high tin content[10,11] and mercury chalcogenides, such as HgTe and HgSe and some of their alloys with Cd, Mn, Fe, and Cr.[1] Interest in such materials has recently been revived, because the parity inversion from Γ_7^+ (odd) to Γ_7^- (even) to Γ_8^+ (odd) with increasing energy makes them topological insulators.[7,12–14] Giving this manuscript the title *Excitonic absorption in topological insulators* would technically be correct, but also misleading, because none of the special effects observed in topological insulators (except for the parity inversion) are relevant for their interband optical absorption.

The parity inversion has an important consequence. Interband transitions from the Γ_7^- valence band to the Γ_8^+ valence and conduction bands, shown by solid arrows in Fig. 1, lead to a strong absorption peak in the midinfrared spectral region. Such transitions have only recently been observed in α-tin[9] and tin-rich $Ge_{1-x}Sn_x$ alloys.[10] They should also dominate the mid-infrared spectra of other gapless semiconductors but have not yet been reported apparently. Intervalence band transitions from Γ_7^- to Γ_8^{+v} can only be observed in p-type gapless semiconductors or in intrinsic gapless semiconductors at finite temperature to create holes as

Published under an exclusive license by the AVS

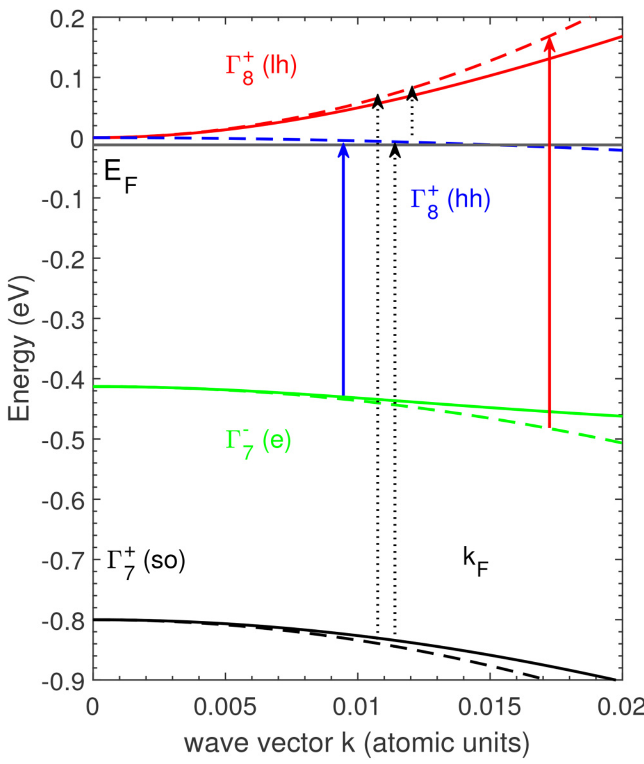

FIG. 1. Band structure of α-tin near the Γ-point from Kane's $8 \times 8\,\vec{k}\cdot\vec{p}$-model (solid) and with parabolic bands (dashed). The symmetry notations in the O_h double group and the equivalent bands for Ge (in parentheses) are also given. Solid and dotted arrows show allowed and forbidden interband transitions, respectively. The horizontal solid line shows the location of the Fermi level at 300 K.

final states for these transitions. Therefore, these transitions are observed in experiments,[9,10] but do not appear in calculated optical spectra, see Fig. 3 in Ref. 5.

Transitions from the Γ_7^+ split-off band to the Γ_8^+ bands or within the Γ_8^+ bands, shown by dotted lines, are forbidden at the Γ-point, but become allowed away from the Brillouin zone center, because their matrix element is linear in k. This has been observed in p-type Ge, GaAs, AlSb, and other semiconductors.[15–18]

A previous article by Carrasco *et al.*[9] only presented a crude analysis of interband transitions in gapless semiconductors, based on the work of Kahn for Ge.[16] The present work describes the model for such transitions in more detail, including degenerate Fermi–Dirac carrier statistics, the excitonic Sommerfeld enhancement, and its screening due to free carriers. The nonparabolicity of the band structure is considered within Kane's $8 \times 8\,\vec{k}\cdot\vec{p}$-model by solving the resulting cubic characteristic equation[1,19] and adjusting the effective masses to reproduce the $\vec{k}\cdot\vec{p}$ band structure. With parabolic bands and established effective masses, the Sommerfeld enhancement is only partially screened at 300 K and excitonic effects lead to an increase of the absorption peak at $\bar{E}_0$. However, the parabolic model underestimates the strength of the absorption

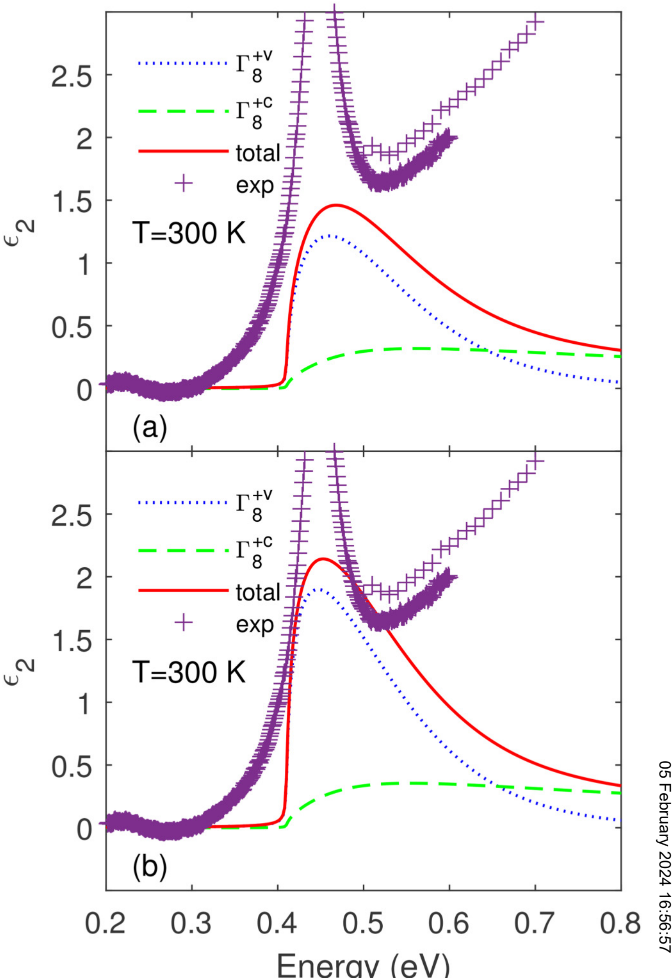

FIG. 2. Contributions to the imaginary part of the dielectric function due to interband transitions from Γ_7^- to Γ_8^{+c} (dashed) and to Γ_8^{+v} (dotted) as well as their sum (solid) in comparison to experimental data from Ref. 9 (symbols), with a constant background determined at 0.2 eV subtracted. Calculated for parabolic bands without (a) and with (b) excitonic enhancement.

peak and does not reproduce the experimental line shape. This discrepancy can be fixed by adjusting the effective masses to better match the $8 \times 8\,\vec{k}\cdot\vec{p}$ band structure.

II. BAND STRUCTURE OF α-TIN

The top three valence bands and the lowest conduction band of α-tin have the following dispersion shown by dashed lines in Fig. 1:

$$E_{8^+c}(k) = +\frac{\hbar^2 k^2}{2m_0 m_{8^+c}}, \tag{1}$$

05 February 2024 16:56:57

Published under an exclusive license by the AVS

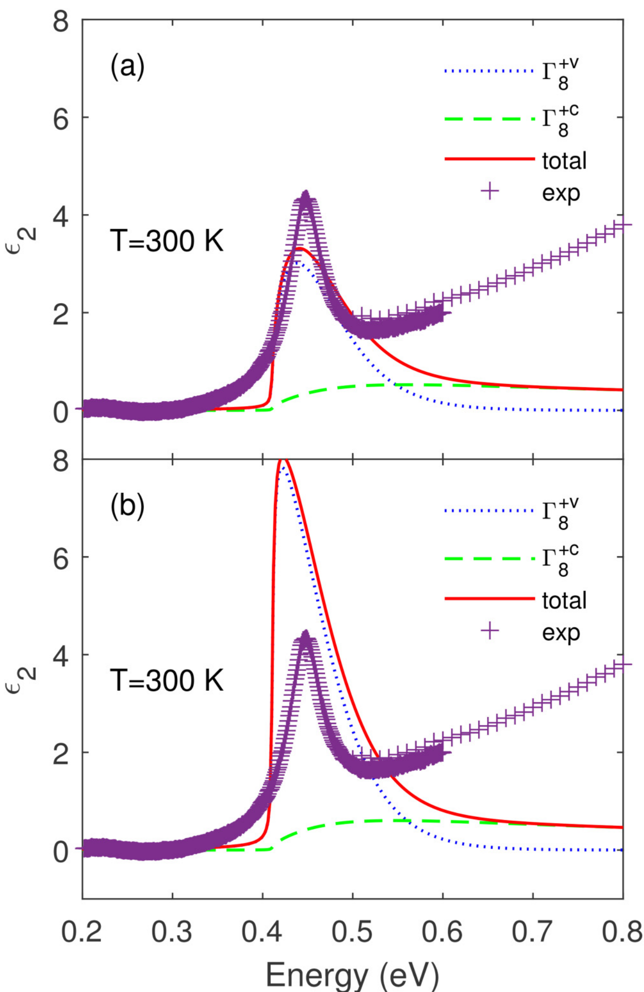

FIG. 3. As Fig. 2, but with effective masses adjusted to account for nonparabolicity without (a) and with (b) excitonic enhancement.

$$E_{8^+v}(k) = -\frac{\hbar^2 k^2}{2m_0 m_{8^+v}}, \tag{2}$$

$$E_{7^-v}(k) = -\bar{E}_0 - \frac{\hbar^2 k^2}{2m_0 m_{7^-v}}, \tag{3}$$

$$E_{7^+v}(k) = -\Delta_0 - \frac{\hbar^2 k^2}{2m_0 m_{7^+v}}, \tag{4}$$

where E_n is the energy of band n, k the wave vector, m_0 the free electron mass in vacuum, and $\hbar$ the reduced Planck's constant. The effective masses are $m_{8^+c} = 0.024$ (p-bonding electron), $m_{8^+v} = 0.26$ (p-bonding heavy hole), $m_{7^-v} = 0.058$ (s-antibonding hole), and $m_{7^+v} = 0.04$ (split-off hole), as given in Table I. These effective masses were determined using magnetoreflection experiments.[20] They are also consistent with $\vec{k}\cdot\vec{p}$-theory.[21] The inverted bandgap $\bar{E}_0 = -E_0$ equals about 0.41 eV, taken as a positive value.[9,10,20,22] The spin–orbit splitting $\Delta_0 = 0.8$ eV is very large.[20] The four conduction band minima at the L-point are expected to be only about 6 meV above Γ at room temperature, nearly degenerate with the Γ_8^+ bands. This difference increases to about 100 meV at low temperatures.[23] See Fig. S1 (Ref. 43) in Ref. 9 for a sketch of the full band structure. The energy reference level is chosen to be where the Γ_8^+ valence and conduction bands touch at the Γ-point.

III. INTERBAND OPTICAL TRANSITIONS

A. Transitions into the Γ_8^{+c} conduction band

Direct interband optical transitions with photon energy $\hbar\omega$ are allowed from the Γ_7^{-v} valence band to the Γ_8^{+c} conduction band, shown by the red arrow in Fig. 1. These bands have the usual curvature, where the initial state band curves downward and the final state band curves upward. The optical (reduced) mass can, therefore, be calculated in the usual way,[21]

$$\mu_c = \frac{m_{7^-v} m_{8^+c}}{m_{7^-v} + m_{8^+c}} = 0.017. \tag{5}$$

Note that we use the subscript c to denote the optical mass for transitions from the Γ_7^- valence band into the Γ_8^{+c} conduction band. These transitions contribute to the dielectric function of α-tin with[24,25]

$$\epsilon_{2,c}(\hbar\omega) = Im \left\langle \frac{A_c}{(\hbar\omega + i\Gamma)^2}\left[2\sqrt{\bar{E}_0} - \sqrt{\bar{E}_0 - \hbar\omega - i\Gamma} - \sqrt{\bar{E}_0 + \hbar\omega + i\Gamma}\right]\right\rangle [f_{7^-v}(\hbar\omega) - f_{8^+c}(\hbar\omega)]. \tag{6}$$

The amplitude prefactor A_c is given by

$$A_c = \frac{e^2\sqrt{m_0}}{3\pi\sqrt{2}\epsilon_0\hbar} E_P \mu_c^{3/2} = 4.918\sqrt{\text{eV}}\, E_P \mu_c^{3/2}, \tag{7}$$

where e is the electronic charge and ϵ_0 the permittivity of vacuum. The $\vec{k}\cdot\vec{p}$ matrix element P is usually expressed through E_P=$2P^2/m_0$, which equals about 24 eV for α-tin.[26] Γ is the broadening parameter for this transition.

The second square-root term in Eq. (6) is nearly imaginary (for small broadening and $\hbar\omega > \bar{E}_0$) and, thus, represents the square rootlike increase of the absorption with photon energy. The first and third square-root terms describe the corresponding contributions to the real part of the dielectric function for $\hbar\omega > \bar{E}_0$.

The last factor in Eq. (6) takes the occupation of the initial and final states for this transition into account. The initial states are all filled, since $\bar{E}_0 \gg k_B T$ and, therefore, we can set $f_{7^-v}(\hbar\omega) = 1$.

05 February 2024 16:56:57

Published under an exclusive license by the AVS

TABLE I. Effective density-of-states masses m_n and reduced (optical) masses μ_n for α-tin, all taken to be positive in units of the free electron mass m_0. The mass at the L-point is for a single L_6^+-valley. From Ref. 9 and calculated as described in the text. The exciton binding energies R_n and radii a_n are also listed. The bandgap $\bar{E}_0$, the momentum matrix element parameter E_P, and the spin–orbit splitting Δ_0 were taken from Ref. 26. The first line lists values for parabolic bands, the second one shows adjustments made to match the $\vec{k}\cdot\vec{p}$ band structure from Fig. 1.

	m_{8^+c}	m_{8^+v}	m_{7^-v}	m_{7^+v}	m_L	μ_c	μ_v	R_c (meV)	a_c (Å)	R_v (meV)	a_v (Å)	$\bar{E}_0$ (eV)	E_P (eV)	Δ_0 (eV)
(p)	0.024	0.26	0.058	0.04	0.19	0.017	0.075	0.4	750	1.8	170	0.41	23.8	0.8
(np)	0.031		0.1	0.053		0.024	0.163	0.6	540	3.8	78			

However, since the bandgap of α-tin is zero, some of the final states in the Γ_8^{+c} conduction band will be occupied through thermal activation (at nonzero temperature). This reduces the strength of the absorption somewhat. This is known as Pauli blocking or band filling. If the last factor is unity, then the real part of ϵ can be obtained analytically by taking the real part of the expression within angular brackets. Otherwise, ϵ_1 needs to be obtained through a numerical Kramers–Kronig transformation, because the Fermi–Dirac factors also depend on photon energy.

The occupation number $f_{8^+c}(\hbar\omega)$ of the final state is found as follows. The photon energy equals the difference between the final and initial band energies (at the same wave vector k for a direct transition). From Eqs. (1), (3), and (5),

$$\hbar\omega = E_f - E_i = E_{8^+c}(k) - E_{7^-v}(k) = \bar{E}_0 + \frac{\hbar^2 k^2}{2m_0\mu_c}. \tag{8}$$

This implies

$$E_{8^+c}(k) = \frac{\hbar^2 k^2}{2m_0 m_{8^+c}} = \frac{\mu_c}{m_{8^+c}}(\hbar\omega - \bar{E}_0). \tag{9}$$

The Fermi occupation factor in the conduction band for the Γ_7^- valence band to the Γ_8^{+c} conduction band transition is, therefore,

$$f_{8^+c}(\hbar\omega) = f\left[\frac{m_{7^-v}}{m_{7^-v}+m_{8^+c}}(\hbar\omega - \bar{E}_0)\right], \tag{10}$$

where $f(E)$ is the Fermi–Dirac distribution function,

$$f(E) = \frac{1}{\exp\left(\frac{E-\mu}{k_B T}\right)+1} \tag{11}$$

with the chemical potential μ (see more below), Boltzmann constant k_B, and temperature T.

B. Transitions into the Γ_8^{+v} valence band

Similarly, transitions from the Γ_7^- valence band to the Γ_8^{+v} valence band, shown by the blue arrow in Fig. 1, are also allowed, but we need to consider that both bands curve downward. The difference between the final and initial state energies is

$$\begin{aligned}\hbar\omega = E_f - E_i &= -\frac{\hbar^2 k^2}{2m_0 m_{8^+v}} + \bar{E}_0 + \frac{\hbar^2 k^2}{2m_0 m_{7^-v}} \\ &= \bar{E}_0 + \frac{\hbar^2 k^2}{2m_0}\left(\frac{1}{m_{7^-v}} - \frac{1}{m_{8^+v}}\right).\end{aligned} \tag{12}$$

The corresponding optical mass for this Γ_7^{-v} to Γ_8^{+v} transition is, therefore,

$$\mu_v = \frac{m_{7^-v} m_{8^+v}}{m_{8^+v} - m_{7^-v}} = 0.075. \tag{13}$$

Transitions can only happen if the photon energy $\hbar\omega$ is larger than the gap $\bar{E}_0$, because the curvature (effective mass) of the Γ_8^{+v} valence band is smaller (larger) than that of the Γ_7^{-v} valence band. The contribution to the dielectric function for this Γ_7^{-v} to Γ_8^{+v} transition is then given by[24,25]

$$\begin{aligned}&\epsilon_{2,v}(\hbar\omega) = Im \\ &\left\langle \frac{A_v}{(\hbar\omega + i\Gamma)^2}\left[2\sqrt{\bar{E}_0} - \sqrt{\bar{E}_0 - \hbar\omega - i\Gamma} - \sqrt{\bar{E}_0 + \hbar\omega + i\Gamma}\right]\right\rangle \\ &[f_{7^-v}(\hbar\omega) - f_{8^+v}(\hbar\omega)],\end{aligned} \tag{14}$$

with the amplitude factor similar to Eq. (7),

$$A_v = \frac{e^2\sqrt{m_0}}{3\pi\sqrt{2}\epsilon_0\hbar} E_P \mu_v^{3/2} = 4.918\sqrt{\text{eV}}\, E_P \mu_v^{3/2}. \tag{15}$$

We again set $f_{7^-v}(\hbar\omega) = 1$, since the Γ_7^{-v} valence band is fully occupied. For intrinsic α-tin (without donors and acceptors) and at zero temperature, the Γ_8^{+v} valence band is also fully occupied and, therefore, the transitions given by Eq. (14) cannot happen, because the last factor in Eq. (14) vanishes. However, at finite temperatures or in p-type α-tin, the presence of holes in the Γ_8^{+v} valence band will allow optical interband transitions that can contribute to the dielectric function.

For such transitions, the final state energy is obtained with a similar argument as in Eq. (8) as

$$E_{8^+v}(k) = -\frac{m_{7^-v}}{m_{8^+v} - m_{7^-v}}(\hbar\omega - \bar{E}_0) \tag{16}$$

05 February 2024 16:56:57

Published under an exclusive license by the AVS

and the final state occupation factor is, therefore,

$$f_{8^+v}(\hbar\omega) = f\left[-\frac{m_{7^-v}}{m_{8^+v} - m_{7^-v}}(\hbar\omega - \bar{E}_0)\right]. \tag{17}$$

Note the minus signs in comparison to Eq. (10). We are already familiar with the argument of the Fermi–Dirac function from Eq. (2) in Ref. 9, except that Maxwell–Boltzmann statistics was used in the previous paper. It is now our goal to repeat this calculation with degenerate Fermi–Dirac statistics. Therefore, we need to calculate the chemical potential for intrinsic α-tin.

Finally, we should note that expressions (6) and (14) are for band-to-band transitions. Excitonic effects have been ignored. We need to reconsider the importance of excitonic effects and screening, once the electron and hole concentrations have been calculated from the chemical potential.

C. Other intervalence band transitions

Transitions from the Γ_7^{+v} split-off valence band to the Γ_8^{+v} valence band or to the Γ_8^{+c} conduction band, shown by the long dotted arrows in Fig. 1, are forbidden at k=0, because the matrix element for these transitions is linear in k. They can occur, however, for nonzero wave vectors k, similar to the intervalence band transitions in p-type Ge, GaAs, GaSb, AlSb, etc. These transitions may cause a change of the slope of ϵ_2 in α-tin at an energy equal to the spin–orbit splitting Δ_0 (see Ref. 16).

Transitions from the Γ_8^{+v} valence band to the Γ_8^{+c} conduction band, shown by the short dotted arrow in Fig. 1, are also forbidden at k=0, because the matrix element is linear in k. They have been observed in other semiconductors,[15–18] but they occur at energies much lower than $\bar{E}_0$ in α-tin and, therefore, cannot impact the line shape of the peak at $\bar{E}_0$.

IV. FERMI–DIRAC INTEGRALS

To calculate the chemical potential and the electron and hole densities for intrinsic α-tin as a function of temperature, we will need the Fermi–Dirac integrals,[27]

$$F_n(x) = \frac{1}{\Gamma(n+1)}\int_0^\infty \frac{y^n}{\exp(y-x)+1}dy, \tag{18}$$

where $\Gamma(n)$ is the Γ-function. Specifically for $n=\frac{1}{2}$ and $n=\frac{3}{2}$, we have

$$F_{1/2}(x) = \frac{2}{\sqrt{\pi}}\int_0^\infty \frac{\sqrt{y}}{\exp(y-x)+1}dy \quad \text{and} \tag{19}$$

$$F_{3/2}(x) = \frac{4}{3\sqrt{\pi}}\int_0^\infty \frac{y\sqrt{y}}{\exp(y-x)+1}dy. \tag{20}$$

Note the prefactors before the integrals, which are not always found in the older literature.

Following Ulrich *et al.*,[27] Fermi–Dirac integrals can be calculated from standard special functions called polylogarithms,

$$Li_m(x) = \frac{1}{\Gamma(m)}\int_0^\infty \frac{t^{m-1}}{x^{-1}\exp(t)-1}dt, \tag{21}$$

which are defined for all x and any integral or nonintegral order $m > 0$. Using polylogarithms with negative arguments expressed as an exponential, the Fermi–Dirac integrals can be calculated as

$$F_n(x) = -Li_{n+1}[-\exp(x)], \tag{22}$$

for $n > -1$. Polylogarithms are called in MATLAB (Ref. 28) with the Symbolic Math Toolbox as Li=polylog(n,x), where n is the order and x the argument of the polylogarithm function.

For large negative arguments $x \ll -1$, one can use the approximation,[29,30]

$$F_n(x) \approx \exp(x), \tag{23}$$

which is valid for any order n. This approximation corresponds to the nondegenerate (classical) limit, where the Fermi–Dirac distribution is replaced with the Maxwell–Boltzmann distribution. There are also approximations for the completely degenerate case $x \gg 1$, where the Fermi–Dirac integral can be replaced by a power of the argument, for example,[29,30]

$$F_{\frac{1}{2}}(x) \approx \frac{4}{3\sqrt{\pi}}x^{\frac{3}{2}}. \tag{24}$$

For $x=0$, the Fermi–Dirac integral is related to Riemann's zeta-function[29] and the Dirichlet eta-function. Unfortunately, no suitable expansion exists for $x \approx 0$ (see Ref. 29), which is needed for our purposes (see below), where k_BT is much greater than the magnitude of the chemical potential and the energies of holes and electrons in the Γ_8^+ bands.

V. CALCULATION OF THE CHEMICAL POTENTIAL AND INTRINSIC CARRER CONCENTRATION

The hole density for intrinsic (undoped) α-tin as a function of temperature is[31]

$$\begin{aligned} p(T) &= \int_{-\infty}^{0} dE\, g_v(E)\,[1-f(E)] \\ &= \int_{-\infty}^{0} dE\, g_v(E)\,\frac{1}{\exp[(\mu-E)/k_BT]+1}, \end{aligned} \tag{25}$$

where[31]

$$g_v(E) = \frac{(m_0 m_{8^+v})^{3/2}}{\hbar^3\pi^2}\sqrt{-2E} \tag{26}$$

is the density of states of holes in the Γ_8^{+v} band for negative energies E. With the substitution $x=-E/k_BT$, the hole density

05 February 2024 16:56:57

Published under an exclusive license by the AVS

TABLE II. Chemical potential μ at different temperatures T for intrinsic α-tin, calculated by equating Eqs. (27) and (28). The hole and electron concentrations in the Γ and L-valleys are also given. The Hulthén parameters g for transitions to the Γ_8^{+v} and Γ_8^{+c} bands obtained from Eq. (37) are also given. This calculation was performed for parabolic (p) and nonparabolic (np) bands.

T (K)	μ (meV)	p (10^{18} cm^{-3})	n_Γ (10^{18} cm^{-3})	n_L (10^{18} cm^{-3})	$g_v(\Gamma_8^{+v})$	$g_c(\Gamma_8^{+c})$
4 (p)	0.8	0.0004	0.0004	0	2.21	0.50
10 (p)	2	0.003	0.002	0.001	1.48	0.34
100 (p)	−2	0.61	0.01	0.60	0.31	0.07
300 (p)	−12.5	3.67	0.05	3.62	0.22	0.05
300 (np)	−12.6	3.68	0.07	3.61	0.47	0.05

becomes[31,32]

$$p(T) = \frac{1}{4}\left(\frac{2m_0 m_{8^+v} k_B T}{\pi\hbar^2}\right)^{3/2} F_{1/2}\left(-\frac{\mu}{k_B T}\right) = P_{8^+v}(T) F_{1/2}\left(-\frac{\mu}{k_B T}\right). \quad (27)$$

This expression assumes that the Γ_8^{+v} hole bands are parabolic and spherical. Nonparabolicity could be added with the $F_{3/2}$ Fermi integrals, but is probably not important for the Γ_8^{+v} hole bands. To take into account the warping of the heavy hole bands, a density of states mass m_{8^+v} must be inserted for the holes.

The electron density is also written as a density-of-states integral as in Eq. (25), but this is more difficult to express, because of the near degeneracy of the Γ_8^{+c} and L_6^+ conduction band minima. We use a multicarrier model similar to what was written for Ge,[25] where electrons can also be present in several conduction band minima at Γ and L,

$$n(T) = 4N_L(T) F_{1/2}\left(\frac{\mu - E_{\text{ind}}}{k_B T}\right) + N_{8^+c}(T) F_{1/2}\left(\frac{\mu}{k_B T}\right), \quad (28)$$

$$N_L(T) = \frac{1}{4}\left(\frac{2m_0 m_L k_B T}{\pi\hbar^2}\right)^{3/2}, \quad (29)$$

$$N_{8^+c}(T) = \frac{1}{4}\left(\frac{2m_0 m_{8^+c} k_B T}{\pi\hbar^2}\right)^{3/2}. \quad (30)$$

The density of states factors $N_c(T)$ and $P_v(T)$ have been defined in the usual way.[31,32] The prefactor 4 of the first term in Eq. (28) is the number of nonequivalent L-valleys. m_L=0.19 is, therefore, the density of states mass for a single L-valley, see Table I. One could take the nonparabolicity of the Γ_8^{+c} valley into account with an $F_{3/2}$ Fermi function,[23,25] but we did not implement that. Instead, we incorporate the nonparabolicity of the Γ_7^- valence band and the Γ_8^+ conduction band with a slight modification of the effective masses to better match the $8 \times 8\, \vec{k} \cdot \vec{p}$ band structure shown in Fig. 1. $E_{\text{ind}} = 6$ meV is the energy of the L-valleys above the reference level.[23]

We can evaluate the prefactor[32]

$$\frac{1}{4}\left(\frac{2m_0 k_B}{\pi\hbar^2}\right)^{3/2} = 4.8294 \times 10^{15}\,\text{cm}^{-3} K^{-3/2} \quad (31)$$

by expressing one factor $\hbar$ in Joules to cancel the kilogram units, the other one in electron volts to cancel the Boltzmann constant expressed in eV/K.

In an intrinsic semiconductor, the charge neutrality requires the number of electrons to be equal the number of holes. We can, therefore, set Eq. (27) equal to Eq. (28). For each temperature T, this yields an equality that can be solved for the chemical potential to yield $\mu(T)$ using the MATLAB (Ref. 28) fzero() function. Table II shows the Fermi level for intrinsic α-tin and the occupations of the various bands at several temperatures **for a constant value** of the indirect gap $E_{\text{ind}} = 6$ meV. This could be modified by introducing a temperature dependence.[23]

At room temperature, $k_B T$ is much larger than the separation E_{ind} between Γ- and L-minima in the conduction band. Electrons are, therefore, mostly found in the L-minima because of their large density of states. The hole density of states is smaller than the L-electron density of states and, therefore, the Fermi level is negative. The overall intrinsic electron and hole density at room temperature is about 3.7×10^{18} cm^{-3}. At low temperatures, electrons are located in the Γ_8^{+c} valley, which has a very small density of states, smaller than that of the Γ_8^{+v} hole band. The Fermi energy is, therefore, positive. The carrier concentration is only 3×10^{15} cm^{-3} at 10 K, three orders of magnitude smaller than at room temperature.

The Γ_7^{-v} valence band and its shape do not enter into the calculation of the chemical potential, because it is always fully occupied. The nonparabolicity of the Γ_8^{+c} conduction band, while significant, should not matter either, because the electron density (28) is dominated by the L-valleys at room temperature. The impact of the L-valley nonparabolicity is probably also small, based on Hall effect data for α-tin[23] and calculations for Ge.[33] The Γ_8^{+v} heavy hole band is quite parabolic in similar semiconductors, but warped.[34] A density-of-states mass (averaged over all directions in $\vec{k}$-space) must be used for this band. All things considered, our carrier concentration and chemical potential at room temperature are probably about as accurate as the m_L and m_{8^+v} effective masses, despite the application of parabolic bands. Our calculated value of $p = 3.67 \times 10^{18}$ cm^{-3} at 300 K agrees well with electrical Hall effect measurements.[23]

05 February 2024 16:56:57

Published under an exclusive license by the AVS

VI. MOTT TRANSITION AND SCREENING OF EXCITONIC EFFECTS

To determine if excitonic effects play a role in the optical interband transitions near $\bar{E}_0$ for intrinsic α-tin, we start by calculating the electron density at the Mott transition. The exciton binding energy in α-tin formed by Γ_7^{-v} holes with Γ_8^{+v} or Γ_8^{+c} electrons is[35]

$$R_{v,c} = \frac{\mu_{v,c}}{\epsilon_\infty^2} R_H, \tag{32}$$

where $R_H = 13.6$ eV is the binding energy of the hydrogen atom and ϵ_∞=24 is the static dielectric constant[9] (which is the same as the high-frequency dielectric constant for diamondlike semiconductors, because there are no infrared-active phonons). The optical masses $\mu_{c,v}$ are given in Table I. The corresponding excitonic Bohr radii are given by

$$a_{v,c} = \frac{\epsilon_\infty}{\mu_{v,c}} a_H, \tag{33}$$

where $a_H = 0.529$ Å is the Bohr radius of the hydrogen atom. The exciton parameters are also given in Table I.

For the moment, we choose a Mott criterion (with a more precise criterion given later),

$$r_s = \frac{1}{a_n}\sqrt[3]{\frac{3}{4\pi n_M}} \sim 1, \tag{34}$$

where a_n is the excitonic radius given by Eq. (33). This implies a Mott density,

$$n_M = \frac{3}{4\pi} a_n^{-3}, \tag{35}$$

which comes out to 4.9×10^{16} cm^{-3} for Γ_8^{+v} excitons and 5.7×10^{14} cm^{-3} for Γ_8^{+c} excitons. The intrinsic charge density of α-tin at room temperature is much higher (3.67×10^{18} cm^{-3}, see Table II) and, therefore, the excitonic enhancement of the Γ_7^- to Γ_8^{+v} and Γ_8^{+c} transitions is at least partially screened.

To quantify this statement, we calculate the Debye–Hückel screening wave vector,[36]

$$k_D = \sqrt{\frac{pe^2}{\epsilon_0 \epsilon_\infty k_B T}} = \sqrt{\frac{p}{\epsilon_\infty T}} \times \sqrt{0.021\ \text{Kcm}}, \tag{36}$$

and the Hulthén parameter,[37]

$$g = \frac{12}{\pi^2 a_n k_D} = \frac{12}{\pi^2 a_n}\sqrt{\frac{\epsilon_0 \epsilon_\infty k_B T}{pe^2}}. \tag{37}$$

One would typically add a factor of 2 in the numerator of Eq. (36) to account for screening of the excitonic interaction by free electrons and holes,[38] but at room temperature, most electrons in α-tin are at the L-valley and they probably do not contribute to the screening of direct excitons at the Γ-point. At room temperature with the carrier concentration given in Table II, we find a Debye screening wave vector of 0.0327 Å^{-1} (or a Debye screening length $\lambda_D = 1/k_D$ of 31 Å, much smaller than the excitonic radii, see Table I). The screening factor g, therefore, equals 0.22 for transitions to the Γ_8^{+v} valence band and 0.05 for transitions to the Γ_8^{+c} conduction band at 300 K. $g = 1$ is typically associated with the Mott criterion and, therefore, we expect the excitonic Sommerfeld enhancements to be screened somewhat in α-tin at room temperature, compare Fig. 5 in Ref. 25.

Tanguy calculated the direct gap absorption of screened excitons,[39]

$$\epsilon_2(\hbar\omega) = Im \left\langle \frac{A_n\sqrt{R_n}}{(\hbar\omega + i\Gamma)^2}\left\{\tilde{g}\left[\tilde{\xi}(\hbar\omega + i\Gamma)\right] + \tilde{g}\left[\tilde{\xi}(-\hbar\omega - i\Gamma)\right] - 2\tilde{g}\left[\tilde{\xi}(0)\right]\right\}\right\rangle [f_h(\hbar\omega) - f_e(\hbar\omega)], \tag{38}$$

$$\tilde{g}(z) = -2\psi\left(\frac{g}{z}\right) - \frac{z}{g} - 2\psi(1-z) - \frac{1}{z}, \tag{39}$$

$$\tilde{\xi}(z) = \frac{2}{\sqrt{\frac{\bar{E}_0 - z}{R}} + \sqrt{\frac{\bar{E}_0 - z}{R} + \frac{4}{g}}}, \tag{40}$$

where A_n is the transition amplitude defined in Eqs. (7) and (15) and R_n the exciton binding energy. $\psi(z)$ is the digamma or psi function, i.e., the logarithmic derivative of the Γ-function, which can be evaluated for complex arguments using the fdigamma.m package in MATLAB.[28] Despite the small Hulthén parameters g, the Sommerfeld enhancement does not disappear completely for the intervalence band transitions and, therefore, the simpler band-to-band expressions (6) and (14) should not be used.[25]

VII. DISCUSSION AND COMPARISON WITH EXPERIMENT

We are now able to evaluate the strength of optical transitions $\epsilon_2(\hbar\omega)$ from the Γ_7^{-v} valence band into the Γ_8^{+c} conduction and Γ_8^{+v} valence bands using Eqs. (6) and (14). We assume an inverted gap of $\bar{E}_0 = 0.41$ eV from Ref. 9 and a broadening parameter Γ of 1 meV, which is typical for direct gap transitions in direct cubic semiconductors.[40] Because of the energy-dependent occupation factors (10) and (17), the real part $\epsilon_1(\hbar\omega)$ needs to be calculated numerically, for example, in *MATLAB* (Ref. 28) using Valerio Lucarini's add-on *Tools for Data Analysis in Optics, Acoustics, Signal Processing*.[41] So far, we have ignored the nonparabolicity of the Γ_8^{+c} conduction band, the Sommerfeld (excitonic) enhancement,[24] and Hulthén screening of excitons.[39] The contribution to the dielectric function from interband transitions at the Γ-point is shown in Fig. 2(a).

05 February 2024 16:56:57

Published under an exclusive license by the AVS

The resulting curves are very similar to those shown in Fig. 3 of Ref. 9. This indicates that the use of degenerate Fermi–Dirac statistics is not important and nondegenerate (Maxwell–Boltzmann) statistics is sufficient to describe these interband transitions. This is surprising since k_BT is several times larger than the chemical potential, see Table II. Therefore, the argument of the Fermi–Dirac integral is close to zero (far from the nondegenerate limit), where no good expansion exists.

Due to the larger reduced mass, transitions to the Γ_8^{+v} (heavy hole) valence band dominate over those to the Γ_8^{+c} conduction band. The onset of absorption occurs at $\bar{E}_0 = 0.41$ eV. The maximum of $\epsilon_2 = 1.46$ is at 0.47 eV, about k_BT larger than $\bar{E}_0$. At lower energies, ϵ_2 is reduced by the joint density of states, at higher energies by the occupation factor. The heavy hole contribution decreases toward larger energies (due to the decreasing occupation factor) more quickly than the Γ_8^{+c} contribution, which is governed by the ω^2-term in the denominator of Eq. (6). The real part ϵ_1 can be calculated from ϵ_2 using Kramers–Kronig transformation, but it does not include contributions from the vacuum ($\epsilon = 1$) and from nonresonant transitions at higher energies.[40]

Equation (38) allows us to study the impact of excitonic enhancement. For completely unscreened excitons and a broadening of $\Gamma = 1$ meV (not shown), there is a strong discrete excitonic peak just below $\bar{E}_0$. The maximum of $\epsilon_2 = 2.5$ is at 0.43 eV. As expected, the maximum is larger than for interband transitions due to the Sommerfeld enhancement. Also, the peak is shifted to lower energies, since the Sommerfeld enhancement decreases for larger energies above the bandgap.[21]

It is more realistic to consider the screening of excitons with the Hulthén parameters g given in Table II, see Fig. 2(b). The maximum $\epsilon_2 = 2.14$ is now at 0.45 eV. As expected, for $g = 0.22$, the Sommerfeld enhancement is only partially screened and, therefore, ϵ_2 is larger and occurs at a lower energy than for the interband case shown in Fig. 2(a).

Overall, all three scenarios (excitonic transitions with full, partial, and no screening) lead to similar results for the dielectric function, except for the discrete exciton peak, which is only present for unscreened excitons. Theory shows that discrete excitonic peaks only exist for $g > 1$, even for small broadenings.[39] All curves show a rather steep rise of ϵ_2 followed by a slow decrease. This is in stark contrast to the experiment, which shows a sharp peak with a steep increase and decrease.[9]

We also varied the value of the indirect gap E_{ind} between ± 50 meV in our calculations. This changes the magnitude of the peak somewhat, but the slow decrease toward higher photon energies remains. Since parabolic bands with established effective masses do not explain the experimental observations, we will discuss in Sec. VIII how nonparabolicity corrections affect these calculations.

VIII. IMPACT OF NONPARABOLICITY

As shown in Fig. 1, the dispersion obtained using the experimental effective masses listed in Table I (dashed lines) does not match the band structure calculated using Kane's $8 \times 8\, \vec{k} \cdot \vec{p}$-model (solid).[19] To achieve a better fit to the band structure on this scale and to consider the nonparabolicity of the bands, we adjust the effective masses to better fit the $8 \times 8\ \vec{k} \cdot \vec{p}$ band structure. This results in the following values: $m_{8^+c} = 0.031$, $m_{7^-v} = 0.1$, and $m_{7^+v} = 0.053$. The Γ_8^{+c} conduction band mass is increased moderately by 29% and the corresponding optical mass μ_c by 41%. The increase of the Γ_7^- mass is much more significant. It increases by 72% and the corresponding optical mass μ_v by 117%.

Table II shows that the chemical potential and the intrinsic carrier concentration do not change much as nonparabolicity corrections are introduced. This was already predicted in Sec. V, because the chemical potential depends mostly on the heavy hole and L-electron mass, which are assumed to be parabolic.

On the other hand, the increase of the optical masses increases the excitonic binding energy and decreases the exciton radius, especially for transitions to the heavy hole band. The Hulthén parameter g_v for transitions to Γ_8^{+v} has more than doubled. The Sommerfeld enhancement is screened much less. This can seen in Fig. 3.

The optical absorption from transitions to the Γ_8^{+c} conduction band is only increased by about 50%–60%, since the optical mass is increased only moderately and the screening parameter g_c does not change at all.

On the other hand, the amplitude of band-to-band transitions to the heavy hole band Γ_8^{+v} has doubled by the introduction of nonparabolicity. The magnitude of its absorption peak shown in Fig. 3(a) nearly matches the experimental peak (especially if the nonresonant background is subtracted). The peak shape, on the other hand, is still not a good match, if the Sommerfeld enhancement is neglected.

If screened excitonic contributions are included, as shown in Fig. 3(b), then the calculated peak magnitude is twice as large as observed in the ellipsometry experiment. The experimental peak shape is also reproduced much better.

It might be possible to achieve even better agreement with experiment by fine-tuning the effective mass of the Γ_7^- valence band but we shall not pursue this here. Effective masses are influenced in $\vec{k} \cdot \vec{p}$ theory by other "remote" bands and also by the epitaxial strain, which is present in our α-tin layers, which are coherently strained on InSb or CdTe substrates.[10] Future work could also focus on including k-dependent optical dipole matrix elements for the allowed and forbidden transitions[19] and understanding the nonresonant background, which might be due to free-carrier absorption or forbidden interband transitions.

05 February 2024 16:56:57

IX. CONCLUSION

The contribution to the dielectric function from interband transitions near the Γ-point in α-tin was calculated using degenerate Fermi–Dirac carrier statistics in the parabolic band approximation. The results are very similar to those shown in Fig. 3 of Ref. 9. Therefore, the use of Eq. (2) in Ref. 9 with nondegenerate Maxwell–Boltzmann statistics was justified and degenerate carrier statistics are not important. Also, the intrinsic carrier concentration at room temperature is very high and, therefore, excitonic effects are weak, but still need to be considered, because the Sommerfeld enhancement persists beyond the Mott transition. The parabolic approximation does not lead to good agreement with experiments, as shown in Fig. 2.

To test the importance of nonparabolicity, the effective masses were adjusted to better match the "exact" bands calculated from

Published under an exclusive license by the AVS

Kane's $8 \times 8 \vec{k} \cdot \vec{p}$-model. This does not change the chemical potential or the intrinsic carrier concentration at 300 K, because they are determined by the heavy hole and L-electron masses, which are assumed to be parabolic. On the other hand, the significant increase of the Γ_7^- valence band mass enhances the interband transitions, increases the exciton binding energy, reduces the exciton radius and, therefore, also the screening, which leads to better agreement with experiment than the parabolic model.

Additional improvements to the theory could be achieved by increasing the number of bands included in the $\vec{k} \cdot \vec{p}$ calculation, considering the impact of k-dependent matrix elements,[19] and by variations of the effective masses due to the epitaxial strain. An important clue can also be found in the dielectric function of InSb,[42] where the impact of the $\vec{k}$-dependence of the optical dipole matrix element and the nonparabolicity of the Γ_7^- band can be studied.

ACKNOWLEDGMENTS

This research was supported in part by the Air Force Research Laboratory Sensors Directorate, through the Air Force Office of Scientific Research Summer Faculty Fellowship Program®, Contract Nos. FA8750-15-3-6003, FA9550-15-0001, and FA9550-20-F-0005. This material is based upon work supported by the Air Force Office of Scientific Research under Award No. FA9550-20-1-0135. This material is based upon work supported by the National Science Foundation (NSF) under Award No. DMR-2235447. Contributions from graduate students Carlos A. Armenta and Sonam Yadav and discussions with José Menéndez are acknowledged. The author is grateful to Arnold M. Kiefer and Bruce Claflin for hosting him in the AFRL Sensors Directorate where part of this work was performed.

AUTHOR DECLARATIONS

Conflict of Interest

The author has no conflicts to disclose.

Author Contributions

Stefan Zollner: Conceptualization (lead); Formal analysis (lead); Funding acquisition (lead); Investigation (lead); Methodology (lead); Software (lead); Visualization (lead); Writing – original draft (lead); Writing – review & editing (lead).

DATA AVAILABILITY

The data that support the findings of this study are available from the corresponding author upon reasonable request. The MATLAB (Ref. 28) code used to calculate the results can be downloaded as supplementary material[43] or from the author's web site http://femto.nmsu.edu.

REFERENCES

[1] I. M. Tsidilkovski, *Electron Spectrum of Gapless Semiconductors* (Springer, Berlin, 1997).
[2] I. M. Tsidilkovski, *Gapless Semiconductors—A New Class of Materials* (Akademie, Berlin, 1988).
[3] T. Brudevoll, D. S. Citrin, M. Cardona, and N. E. Christensen, Phys. Rev. B **48**, 8629 (1993).
[4] M. Rohlfing, P. Krüger, and J. Pollmann, Phys. Rev. B **57**, 6485 (1998).
[5] S. Küfner, J. Furthmüller, L. Matthes, and F. Bechstedt, Nanotechnology **24**, 405702 (2013); **24**, 469501 (2013).
[6] S. Küfner, J. Furthmüller, L. Matthes, M. Fitzner, and F. Bechstedt, Phys. Rev. B **87**, 235307 (2013).
[7] S. Küfner and F. Bechstedt, Phys. Rev. B **91**, 035311 (2015).
[8] U. Middelmann, L. Sorba, V. Hinkel, and K. Horn, Phys. Rev. B **35**, 718 (1987).
[9] R. A. Carrasco, C. M. Zamarripa, S. Zollner, J. Menéndez, S. A. Chastang, J. Duan, G. J. Grzybowski, B. B. Claflin, and A. M. Kiefer, Appl. Phys. Lett. **113**, 232104 (2018).
[10] R. A. Carrasco, S. Zollner, S. A. Chastang, J. Duan, G. J. Grzybowski, B. B. Claflin, and A. M. Kiefer, Appl. Phys. Lett. **114**, 062102 (2019).
[11] M. P. Polak, P. Scharoch, and R. Kudrawiec, J. Phys. D: Appl. Phys. **50**, 195103 (2017).
[12] A. Barfuss *et al.*, Phys. Rev. Lett. **111**, 157205 (2013); **112**, 239903 (2014).
[13] H. Huang and F. Liu, Phys. Rev. B **95**, 201101 (2017).
[14] C.-Z. Xu *et al.*, Phys. Rev. Lett. **118**, 146402 (2017).
[15] W. Kaiser, R. J. Collins, and H. Y. Fan, Phys. Rev. **91**, 1380 (1953).
[16] A. H. Kahn, Phys. Rev. **97**, 1647 (1955).
[17] R. Braunstein, J. Phys. Chem. Solids **8**, 280 (1959).
[18] R. Braunstein and E. O. Kane, J. Phys. Chem. Solids **23**, 1423 (1962).
[19] E. O. Kane, J. Phys. Chem. Solids **1**, 249 (1957).
[20] S. H. Groves, C. R. Pidgeon, A. W. Ewald, and R. J. Wagner, J. Phys. Chem. Solids **31**, 2031 (1970).
[21] P. Y. Yu and M. Cardona, *Fundamentals of Semiconductors* (Springer, Heidelberg, 2010).
[22] S. Groves and W. Paul, Phys. Rev. Lett. **11**, 194 (1963).
[23] C. A. Hoffman, J. R. Meyer, R. J. Wagner, F. J. Bartoli, M. A. Engelhardt, and H. Höchst, Phys. Rev. B **40**, 11693 (1989).
[24] C. Tanguy, Phys. Rev. Lett. **75**, 4090 (1995) ; **76**, 716 (1996).
[25] J. Menéndez, C. D. Poweleit, and S. E. Tilton, Phys. Rev. B **101**, 195204 (2020).
[26] P. Lawaetz, Phys. Rev. B **4**, 3460 (1971).
[27] M. D. Ulrich, W. F. Seng, and P. A. Barnes, J. Comp. Electron. **1**, 431 (2002).
[28] See http://www.mathworks.com.
[29] J. S. Blakemore, Solid State Electron. **25**, 1067 (1982).
[30] R. Kim, X. Wang, and M. Lundstrom, "Notes on Fermi-Dirac integrals," arXiv:0811.0116.
[31] N. W. Ashcroft and N. D. Mermin, *Solid State Physics* (Saunders, Fort Worth, 1976).
[32] S. M. Sze and K. K. Ng, *Physics of Semiconductor Devices* (Wiley, Hoboken, 2007).
[33] C. Xu, J. Kouvetakis, and J. Menéndez, J. Appl. Phys. **125**, 085704 (2019).
[34] G. Dresselhaus, A. F. Kip, and C. Kittel, Phys. Rev. **98**, 368 (1955).
[35] R. J. Elliott, Phys. Rev. **108**, 1384 (1957).
[36] H. Haug and S. W. Koch, *Quantum Theory of the Optical and Electronic Properties of Semiconductors* (World Scientific, Singapore, 2004).
[37] L. Bányai and S. W. Koch, Z. Phys. B **63**, 283 (1986).
[38] L. Pavesi, J. L. Staehli, and V. Capozzi, J. Phys. C **21**, 1485 (1988).
[39] C. Tanguy, Phys. Rev. B **60**, 10660 (1999).
[40] C. Emminger, F. Abadizaman, N. S. Samarasingha, T. Tiwald, and S. Zollner, J. Vac. Sci. Technol. B **38**, 012202 (2020).
[41] V. Lucarini, K.-E. Peiponen, J. J. Saarinen, and E. M. Vartiainen, *Kramers-Kronig Relations in Optical Materials Research* (Springer, Heidelberg, 2005).
[42] M. Rivero Arias, C. A. Armenta, C. Emminger, C. M. Zamarripa, N. S. Samarasingha, J. R. Love, S. Yadav, and S. Zollner, J. Vac. Sci. Technol. B **41**, 022203 (2023).
[43] See the supplementary material online for MATLAB scripts to perform the calculations presented here.

05 February 2024 16:56:57

Published under an exclusive license by the AVS